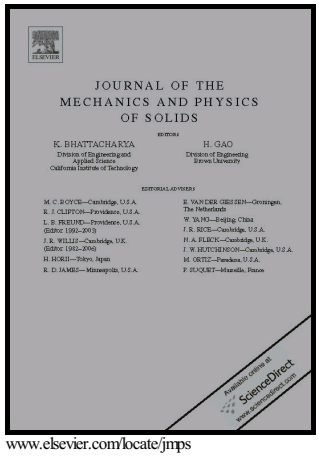

www.elsevier.com/locate/jmps

Separating Plasticity-Induced Closure and Residual Stress Contributions to Fatigue Crack Retardation Following an Overload

Enrico Salvati, Hongjia Zhang, Kai Soon Fong, Xu Song, Alexander M. Korsunsky

PII: S0022-5096(16)30553-1
DOI: http://dx.doi.org/10.1016/j.jmps.2016.10.001
Reference: MPS2993

To appear in: *Journal of the Mechanics and Physics of Solids*

Received date: 7 August 2016
Revised date: 30 September 2016
Accepted date: 4 October 2016

Cite this article as: Enrico Salvati, Hongjia Zhang, Kai Soon Fong, Xu Song and Alexander M. Korsunsky, Separating Plasticity-Induced Closure and Residual Stress Contributions to Fatigue Crack Retardation Following an Overload *Journal of the Mechanics and Physics of Solids* http://dx.doi.org/10.1016/j.jmps.2016.10.001

Separating Plasticity-Induced Closure and Residual Stress Contributions to Fatigue Crack Retardation Following an Overload

Enrico Salvati[1*], Hongjia Zhang[1], Kai Soon Fong[2], Xu Song[2], Alexander M. Korsunsky[1]

[1]Department of Engineering Science, University of Oxford, Parks Road, Oxford, OX13PJ, United Kingdom

[2]SIMTech - Singapore Institute of Manufacturing Technology. 71 Nanyang Dr, Singapore 638075

Corresponding author. Enrico Salvati, Department of Engineering Science, University of Oxford, Parks Road, Oxford OX1 3PJ, United Kingdom. Tel.: +44 18652 73043; fax: +44 18652 73010. enrico.salvati@eng.ox.ac.uk

Abstract

The introduction of an overload or underload within a constant amplitude loading fatigue test leads to a retardation or acceleration of the Fatigue Crack Growth Rate (FCGR). The understanding of the causes of these effects is essential in the context of variable amplitude fatigue loading, since in principle any loading history can be represented as a sequence of overloads and underloads. In the case of overload, along with some other minor causes, the residual stress changes at the crack tip and crack closure behind the tip can be thought of as the main factors that affect the fatigue crack growth rate. Whilst this has been recognised and accepted for many decades, controversy persists regarding the relative significance and presence of these two effects, and consensus is yet to emerge. The effect of crack closure, when the baseline loading ratio is high enough, can be inhibited so that the main cause of retardation becomes doubtless the residual stress present ahead the crack tip.

In the present paper we report our attempt to deconvolve the contributions of crack closure and residual stress on crack retardation following an overload. To accomplish this task we analyse the results of fatigue tests run at two baseline load ratios, namely R=0.1 and R=0.7. At the load ratio of R=0.7 the crack closure effect is not operative, as confirmed by Digital Image Correlation analysis of

the crack flanks close to the tip, and post mortem fractographic analysis of crack surfaces. Therefore, for R=0.7 the compressive residual stress region created by the overload ahead of the crack tip is the sole mechanism causing crack retardation. Therefore, for R=0.7 the focus must be placed entirely on the strain field around the crack tip. To this end, line profiles along the crack bisector of elastic strain in the crack opening direction were collected at several stages of crack propagation past the overload using in situ Synchrotron X-ray Powder Diffraction (SXRPD) technique.

By performing comparison between the two loading conditions (R=0.7 and R=0.1), information was extracted regarding the role of residual stress alone, and then, by subtracting this effect for the R=0.1 sample, for crack closure alone. To enable this analysis, we propose a introducing the concept of equivalent effective stress intensity factor range, $\Delta K_{eq,eff}$ proposed by Walker. Afterwards, the SIF range reduction ratio, β, which represents the "knock down" factor with respect to the steady state growth was assessed. It is in terms of these newly introduced parameters that the magnitude and extent of the overload-induced crack growth rate retardation can be plotted, fitted and decomposed into closure and residual stress effects, respectively. It is concluded that although the residual stress effect is present at all values of the load ratio R, its effect is relatively short-lived, whilst the closure effect that is dominant at low values of R causes longer range retardation.

Graphical abstract

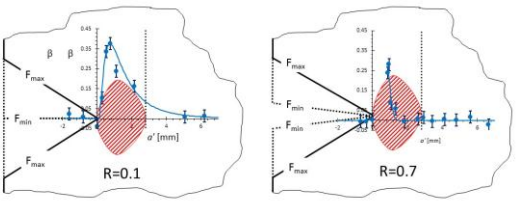

Keywords: crack tip plasticity; fatigue; crack propagation and arrest; crack mechanics; residual stress; overload

1. Introduction

The Fatigue Crack Growth Rate (FCGR) retardation effect due overload has been known for almost fifty years [1, 2]. The causes of such retardation have been imputed to various phenomena that take place during the occurrence of the overload, such as residual stress generation, plastic deformation and the consequent plasticity-induced crack closure, and work hardening. However, no clear consensus has been reached regarding the relative significance of these mechanisms [3-7].

Crack closure is a mechanism active in the wake of the crack that is caused by the plastic deformation-induced modification of the crack flank geometry [8]. Crack closure effect may be operative during crack propagation even in the absence of overload, but becomes particularly significant once an overload has been applied. As the crack tip moves forward past the overload-affected region, during the unloading part of the cycle crack flanks come into contact prior to the cyclic load reaching its minimum value. This results in a lower effective range of crack opening displacement and crack tip stress intensity factor. It is important to note that in the case of overload, closure causes crack retardation only when crack face contact occurs in the wake of the growing crack. As the crack tip moves sufficiently far away, the closure effect becomes negligible. Conversely, if crack arrest is observed immediately after the overload, no crack closure can be present until re-nucleation or propagation takes place. This effect has been subject of numerous studies in the past, and its contribution to crack retardation is widely accepted.

The region of heavy plastic deformation ahead of the crack tip gives rise to a region of compressive residual stress. The occurrence of an overload amplifies this compressive residual stress significantly. It is well known that the presence of compressive residual stress ahead of the crack tip impedes propagation due to the local reduction of the mean stress during fatigue cycling. In the last decade the proliferation of new experimental microscopic techniques (X-ray diffraction, DIC and the

FIB ring-core method) [9-12] enabled direct spatially resolved evaluation of residual stress, and better understanding of its evolution during the relevant phases of propagation in the presence of an overload.

Crack closure and compressive residual stress are not the only mechanisms thought to be involved in crack retardation. Indeed, other causes may appear and play their role depending on the loading condition and material behaviour. In the last decades, many authors have directed effort at the understanding of the conditions when these additional effects may arise.

Crack tip blunting is another retardation mechanism [13]: extensive plastic flow at the crack tip may modify the geometry leading to the consequent crack blunting. The resulting crack tip displays behaviour similar to a rounded notch where finite stress concentration is observed, instead of stress intensification observed at a crack tip. Under such circumstances the fatigue crack growth rate (FCGR) is reduced in comparison with the steady-state conditions. The extreme version of this scenario corresponds to the situation when the crack is blunted to such an extent that a new nucleation site appears at a different location from the previous tip [14]. Crack branching or kinking that takes place in this case is another mechanism that contributes to crack retardation [15-16]. Change in the crack growth direction and/or the creation of small secondary cracks lead to the redistribution of stresses around the crack tip which, in turn, reduces the crack driving force and causes retardation.

Another view of the crack propagation process is to assume that the material ahead of the crack tip through which crack advances experiences cyclic loading, damage and localised failure, giving rise to a connected crack. Depending on the material properties and deformation history, strain hardening may play its role in controlling the crack growth rate. Material hardening generally reduces the ductility of the material with a consequent reduction in the resistance to crack propagation [17]. The general consequence of this effect is to accelerate the fatigue crack growth rate (FCGR). However, in terms of the overall significance for FCGR this may be considered of limited, secondary importance. Unlike plasticity-induced crack closure and the residual stress that exert

direct strong influence on FCGR, secondary effects of the kind enumerated above may only become prominent for specific and particular combinations of material properties, microstructure and overload ratio.

Summarising the above discussion, we conclude that crack closure and residual stress can be considered as the primary causes of FCGR retardation phenomenon. The purpose of the present study is to seek to separate the influence of these two mechanisms. This is first done experimentally, by creating test conditions when the former mechanism (crack closure) is switched off, and only the latter (residual stress) is operative at the crack tip. Secondly, based on the test results and theoretical consideration, the analysis of FCGR around the overload phenomenon is carried out in order to elaborate a quantitative description for the contribution made by each mechanism to the retardation effect.

In order to isolate the contribution of residual stress in crack retardation, a comparative study was carried out of fatigue crack growth rate change following an overload between a high loading ratio (R=0.7) and the commonly used low loading ratio (R=0.1) regimes. Therefore these two loading configuration were used in the present experiments.

The experimental tests were conducted using Compact Tension (CT) specimens of AZ31b magnesium alloy that had been subjected to severe plastic deformation by Constrained Groove Pressing (CGP) to obtain fine-grained microstructure with the typical grain size of the order of 1-2µm. The crack length and the appearance of possible secondary crack branches were monitored via optical imaging using a long-range telescope and digital camera, with the effective pixel size of the order ~0.5µm.

In the high loading ratio fatigue crack growth experiment the effect of plasticity-induced crack closure is inhibited [18], or may be entirely nullified. To confirm that this is the case, in situ digital image correlation (DIC) evaluation of crack opening was performed, and direct evidence of the lack of crack closure was obtained. Further corroborating evidence was sought by analysing the fracture surface using Scanning Electron Microscopy (SEM) as well as regarding the loading case (R=0.1). On

the other hand, the crack retardation effect observed at R=0.1 is due to the combination of residual stress and crack closure and here again this is confirmed by DIC and fractography.

Furthermore, the quantification of the strain distribution ahead of the crack tip during the overload application was conducted by means of Synchrotron X-ray Powder Diffraction (SXRPD) for the loading ratio of R=0.7. Experimental measurements were then used to validate further an elasto-plastic 3D FEM model previously adopted by the authors for the study of the crack acceleration induced by an Underload [19]. The numerical model was used to perform the evaluation of the strain state arising as a consequence of OL for the case of R=0.1. Using this model, the juxtaposition between the two considered load ratios was then assessed.

Comparing the FCGR obtained in the two loading ratio cases (R=0.7 and R=0.1), it was possible to carry out careful analysis of the difference in the crack retardation effect as the crack extends. Firstly, a modification of Walker's model [20] allowed the attribution of the unique equivalent SIF range to describe FCGR behaviour for any positive loading ratio. This approach opened the way to presenting the experimental outcomes in a form that is independent of the loading ratio. The deviation from the steady state value of the equivalent SIF range after the overload application is considered as a measure of the magnitude and extent of the crack growth retardation effect. Using the effective SIF range reduction ratio β, the sole influence of residual stress is considered at R=0.1, and the effect of closure could also be isolated by considering the difference between the R=0.1 and R=0.7 results.

2. Material description and Fatigue tests

The material sought for conducting the various experiments reported in this paper required to have specific combination of properties. Above all, good ductility was sought to give a large plastic region at the crack tip and in which residual stress is accommodated. Secondly, since SXRPD technique was to be used for residual stress evaluation, fine-grained material was required to give good compromise between high spatial resolution and good grain averaging and sampling statistics.

For the reasons listed we chose to focus our attention on the magnesium alloy AZ31b treated using a severe plastic deformation processing route that lead to grain refinement and strengthening in combination with good ductility. The resulting grain size varied in the range from 1μm to 5 μm, yield stress of the order σ_y=262MPa and maximum elongation of 10%.

Fatigue tests were performed on CT specimens machined from a 2mm-thick plate with the in-plane dimensions depicted in Fig.1a.

Cyclic load was applied to the sample by means of a servo-hydraulic testing machine at frequencies of 7÷10hz. Static loading for in situ strain mapping using SXRPD was applied using a 5kN Deben® machine. Crack tip opening displacement measurement was used as a means of cross-validation between the two loading arrangements, to ensure that the loading conditions ahead of the crack tip were consistent between the two experimental configurations.

Two fatigue experiments at constant loading ratios of R=0.1 and R=0.7 were conducted, and a single peak overload (OL) was applied in both. The loading histories for both experiments are reported in Fig. 1b and 1c. Both experiments show the same magnitude of maximum force (F_{max}=866.7N) and the overload force (F_{OL}=1300N) that was 50% in excess of the maximum cyclic load, meaning that the overload ratio was R_{OL}=1.5. To achieve the required loading ratios, the lower cyclic load imposed was F_{min}=606.7N for R=0.7, and was F^{I}_{min}=86.7N for R=0.1. The single anomalous overload peak was applied at the crack length of a=9.05mm for the R=0.1 sample, and at a=9.03mm for the R=0.7 sample, respectively. Further fatigue crack growth experiment was conducted beyond the overload until the prevailing trend in the FCGR was re-established.

3. Fatigue Crack Propagation Analysis

3.1 Experimental result

Crack growth rate retardation was observed in both samples. The diagram of crack length versus the number of cycles is plotted in Fig.2. The change in the trend towards slower growth rates is apparent in the propagation past the OL. The fitting lines in Fig.2 indicate the local discontinuities in the FCGR and the apparent shift in the steady-state growth trend.

It worth noting that the experiment at R=0.7 manifests a complete arrest of crack propagation, unlike the R=0.1 case. Re-nucleation occurred after 2500 further cycles past the OL. This behaviour is evident in Fig.2b: right after the OL the crack length plot becomes horizontal, and only departs once the crack re-nucleates, eventually approaching the steady state crack growth trend.

Stress Intensity Factor (SIF) values for FCGR curve construction were evaluated using the equation for a compact tension specimen provided by Murakami [21]:

$$K_I = \frac{F}{b}\sqrt{\frac{\pi}{W}}\left[16.7\left(\frac{a}{W}\right)^{\frac{1}{2}} - 104.7\left(\frac{a}{W}\right)^{\frac{3}{2}} + 369.9\left(\frac{a}{W}\right)^{\frac{5}{2}} - 573.8\left(\frac{a}{W}\right)^{\frac{7}{2}} + 360.5\left(\frac{a}{W}\right)^{\frac{9}{2}}\right] \quad (1)$$

Fig.3 presents crack propagation data in the form of crack growth rate as a function of crack length (Fig.3). The OL-induced retardation is apparent from the drop of the growth rate da/dn at OL, followed by the gradual return to the steady-state rate. Assuming that the crack growth rate gets fully restored once the crack reaches the unaltered material zone, the FCGR curve can be described analytically in accordance with Paris' Law (2):

$$\frac{da}{dn} = C\,\Delta K^m \quad (2)$$

The coefficients C and m are listed in Table 1.

3.2 Walker's model

The idea of mean stress effect correction that was introduced by Walker [20], after previously been widely adopted in the context of stress-life curves [22-24], has been successfully applied in the context of fracture mechanics [25-26].

Walker introduced an equivalent parameter ΔK_{eq} to describe the FCGR for any combination of maximum SIF K_{max} and minimum SIF K_{min} that can be expressed in terms of the load ratio R≥0. The equivalent SIF range ΔK_{eq} is defined as follows:

$$\Delta K_{eq} = K_{max}(1-R)^{\gamma}. \quad (3)$$

Here γ is a measure of material-specific FCGR sensitivity to the mean stress that ranges between 0 and 1. Noting that $\Delta K = K_{max}/(1-R)$, we adopt a way more convenient for the present purpose to express equation (3) directly in terms of the SIF range:

$$\Delta K_{eq} = \Delta K(1-R)^{\gamma-1} \quad (4)$$

Considering the expression for fatigue crack growth rate given by the Paris law as the particular case of R=0, we write:

$$\left(\frac{da}{dN}\right)_{R=0} = C_0\,\Delta K^{m_w} \quad (5)$$

Where C_0 and m_w are the material constants, and subscript w refers to the use of the Walker parameter. Based on the above, expression for the general case is obtained by substituting equation (4) into (5), replacing ΔK with ΔK_{eq}:

$$\frac{da}{dN} = C_0\,[\Delta K(1-R)^{\gamma-1}]^{m_w} \quad (6)$$

This formulation provides a description of the FCGR at any positive load ratio R≥0 in terms of three constants: γ, C_0, m_w. Those constants can be obtained by means of a linear regression using the logarithmic form of (6), as follows:

$$log\left(\frac{da}{dN}\right) = log(C_0) + m_w\, log(\Delta K) + m_w(\gamma - 1)\, log(1 - R) \quad (7)$$

The fitting procedure was applied to the set of experimental data presented here in the crack propagation regime unaffected by the OL, as represented by the dashed line in Figure 3. The material parameters were found to be: $\gamma = 0.649,\ C_0 = 3.34 \times 10^{-10} \frac{m}{cycle\, MPa\, \sqrt{m}},\ m_w = 2.95.$

4. Crack Closure evaluation

4.1. DIC analysis

The presence of plasticity-induced crack closure during the fatigue test was verified using DIC. This method has been successfully adopted in the past [9, 27] and shown to be an efficient way to evaluate the relative displacement of crack flanks during cyclic loading. The tracking points can be positioned along the crack wake so that the closure effect is evaluated as function of position from the crack tip. The necessary requirements for the correct elaboration of peak tracking using DIC is the adequate image resolution and the presence of small features that ensure brightness variation within the image and allow peak tracking. The image acquisition system consisted of a Questar long range telescope attached to a camera having with 640x240 pixel resolution, and an effective pixel size of 1µm for the actual setup used.

The presence of crack closure was verified before and after the application of the OL. For both the loading conditions (R=0.1 and R=0.7), a sequence of images was acquired once the crack had

propagated past the overload position for further 0.55mm. The tracking points were positioned at several locations behind the crack tip, namely, at 25μm, 100μm, 200μm and 400μm.

The acquisition was run at the reduced loading frequency of 0.2 Hz and the frame rate of 4 frames per second, to avoid image blurring. Thus, each cycle was described by ~20 images. The software used for DIC measurement was that developed by Eberl et al. [28].

The evaluated relative displacement plots, with zero opening corresponding to the closed crack condition, are reported in Fig.4 with the applied external load plotted on the vertical axis.

The DIC analysis allows unequivocal identification of the conditions for crack closure to be present during crack growth past an OL.

Figure 4(a) shows that even the absence of anomalous loads, crack closure is present under cyclic fatigue loading at R=0.1. All measurements reveal that crack flank contact occurs before the external load reaches the minimum value, resulting in a deviation from the linear unloading trend. As expected, the effect becomes milder at larger distances from the crack tip. Considering the instant following the OL, the most evident observation that can be made concerns the closure load. The application of the OL reduces the load range over which the crack remains open compared to the sample before the OL. It can be once again noted that at positions further back from the crack tip, the evidence of the closure effect becomes less pronounced.

The closure phenomenon represents a significant reduction of the effective SIF range experienced by the crack tip, by up to a fourth of the total range. Similarly, subsequent loading from the minimum load does not immediately manifest itself in the crack opening, but only appears when the load reaches about a level similar to the closure load.

Regarding the sample corresponding to R=0.7, no evidence of crack closure is found. Figures 4(c) and 4(d) show that both before and after the OL, the displacements follow a straight line

without any anomalies associated with crack closure. Absence of crack closure was seen even in the very vicinity of the crack tip (~25μm).

In summary, DIC analysis reveals the presence of crack closure induced by the OL only under the loading ratio condition of R=0.1. In contrast, adopting R=0.7, i.e. high value of F_{min} inhibits possible crack flank contact.

Let us analyse the effect that crack closure had on the reduction in effective stress intensity factor range for the experiment at R=0.1. Considering the displacement plots shown in Fig.4, the reduction in the SIF acting at the crack tip once the crack closure is active can be evaluated. Assuming a linear relation between load and the crack tip SIF, the following assessment can be made:

$$\alpha = \frac{F_{op}}{F_{max}} = \frac{K_{op}}{K_{max}} \tag{8}$$

Here α is the ratio between the maximum load and the load required for opening the crack (subscript op).

The effective SIF range acting at the crack tip can therefore be evaluated as follows:

$$\Delta K_{eff} = \Delta K\,(1 - \alpha) \tag{9}$$

The effective stress intensity factor taking into account the crack closure effect is defined as:

$$\Delta K_{eff} = K_{max} - K_{op} \tag{10}$$

The record of the loading history during image acquisition allowed the determination of the load level for crack opening. Averaged values of the opening load were assessed over the crack

lengths measured (i.e. up to 0.4mm). The solution of the (8) provided α_{after}=0.35 and α_{prior}=0.18 prior and after the OL introduction, respectively. The physical meaning of α is the reduction of the stress intensity factor range when the crack closure is operative. Using equation (9) it is possible to evaluate the value of the effective range of stress intensity factor at the crack length analysed by DIC. This value can be computed both prior and after the OL application. These turned out to be respectively $\Delta K_{eff,bef}$=12.5 MPa √m and $\Delta K_{eff,aft}$=9.9 MPa √m.

4.2. Fractography

Further insights into the crack propagation mechanism can be obtained through fracture surface analysis using SEM imaging at variable magnification to allow the exploration of the morphology of asperities left by material rupture at several length scales.

The two samples considered in this study were examined with particular attention focused at the overload site. Figures 5(a) and 5(b) provide overview images of the crack surface at the zone of interest. The dashed lines in figures indicate the crack front at the instant of overload application. The crack front profile clearly does not follow a straight line due to the difference in constraint between the bulk and the free surface. Although no analytical solution is available for describing this phenomenon quantitatively, it is well known to be highly dependent on the Poisson's ratio [29]. This three-dimensional effect induces a variation of SIF at the crack front as a function of position across the sample's thickness.

Comparing the two images, an observation can be made that the enhanced plastic deformation is present in the sample (R=0.1) at the vicinity of the free surfaces along the through thickness z direction (highlighted in red). This is associated with the change in the stress state (principal stresses in particular), as studied numerically and reported in the literature [30]. In contrast, the same observation cannot be made readily for the sample fatigued at R=0.7, since no evident plastic deformation "lip" is evident. Furthermore, higher magnification imaging at these deformed areas

(site c) reveals another interesting aspect shown in Figure 5(c). The surface roughness at site "c" is visibly different compared to site d. A possible explanation for this observation is that crack closure was operative within the highlighted near-surface region during crack propagation past the overload. This is in agreement with previously reported studies [30] that suggest high values of crack opening stress intensity factors to be found for locations lying nearby the free surface. The hypothesis that we put forward (and that allows additional corroboration) is that crack closure modifies the apparent roughness of the fracture as consequence of repeated contact between crack flanks during cycling. It has been argued in the literature that the region of material that undergoes contact due to crack closure should not depend upon sample thickness [31], unless the thickness is comparable with the closure zone size. Note that the fact that no apparent crack closure occurred during the loading ratio R=0.7 test is corroborated by Figure 5(b) that does not show any altered zone at all.

Finally, the change of crack surface morphology due to the overload proper is shown in Fig.5(e). The higher topology of the central "ridge" in the image corresponds to the large plastic deformation that causes closure and leads to the consequent change in the FCGR observed in the experiment.

5. Strain field evolution

5.1. Experimental measurements using SXRPD

Synchrotron X-ray Powder Diffraction (SXRPD) is a powerful tool for spatially resolved strain studies in polycrystalline materials. Since high energy, high flux X-ray beams are required for mapping the lattice parameter variation in the bulk of load-bearing components, synchrotron-based instruments are often used. During the past decade successful use of this technique has been reported for crack tip stress/strain evaluation [9-12, 18, 32-33].

The experiment reported here was aimed at spatially resolved residual strain evaluation along the crack extension line within the sample, at four different stages of crack propagation, with respect to the load application history. In terms of the crack retardation due to overload, in the sample tested at R=0.7 (analysed by SXRPD) this effect is expected to be caused uniquely by the compressive residual stress, whereas in the R=0.1 sample, a combination of crack closure and residual stress retardation is present. The purpose of the synchrotron-based experiment was therefore to measure the evolution of the near-tip strain (stress) state using SXRPD technique.

Experiment was conducted on the I15 beamline at Diamond Light Source (DLS, Harwell, UK). X-ray energy was set to 76.6keV, with the beam size defined by collimating slits as 45x45µm. In situ sample loading was provided by a 5kN Deben© portable stage that was mounted on a diffractometer able to accomplish movements along the x',y' and z' axes, as indicated in Fig.6. The test was performed in transmission mode, and it was assumed that out-of-plane stresses are negligible (plane stress approximation). A series of complete Debye-Sherrer rings was acquired using a PerkinElmer flat panel 1621-EN detector (2048x2048 pixels, pixel size 0.2x0.2mm^2) placed on the axis of the incoming beam, as shown in Fig.6. The sample-detector distance was adjusted to obtain an optimum combination of coverage and positional precision for the rings of interest.

Referring to Fig.1c which shows the loading history, spatially resolved strain line profiling was performed at the instants denoted as B, OL, C and D. The line scan step adopted was equal to the X-ray beam spot size (45µm), and each line scan covered approximately 2mm in length ahead of the crack tip.

For the purposes of strain analysis, the (101) Debye-Scherrer ring was subjected to radial binning performed to extract the equivalent 1D X-ray diffraction profile for scattering in the direction parallel to the load application. The lattice spacing variation Δd was then evaluated throughout the scan, for use in the differential form of Bragg's law to determine strain, as follows:

$$\varepsilon_{yy} = \frac{\Delta d}{d_0} \quad (11)$$

As it is well known, determination of strain using the above formula requires the knowledge of strain-free lattice parameter d_0. Defining this parameter often presents a practical challenge, since finding an appropriate unstrained location within or outside the sample is not always possible. A rough assessment, considering a stress-free region of the sample, was made. Afterwards, further refinement was performed by comparison and subsequent matching with the solution given by elastoplastic FEM analysis.

The procedure for precise determination of d_0 was carried out using the set of measurements acquired at step B (Fig.1c), and once d_0 was found by matching with the FEM solution, the remaining line scans were interpreted accordingly. In reference to the coordinate system shown in Fig.1a, yy strain component profiles, from the experimental measurements, at the various stages of crack growth are reported in Fig.7 using markers and dashed curves, together with the FEM solutions shown as continuous lines.

Satisfactory agreement is found between the FEM solution given using nominal load, and SXRPD measurements.

The results reported above confirm the magnification of compressive residual strain due to the OL application. In fact, the strain profile referring to the propagation stage “C” in Fig.7 shows a lower magnitude of strain compared to the propagation stage “B” that identifies the instant prior the OL. Plastic deformation occurring at the crack tip when the OL is operative is far greater than that induced by the cyclic loading, when the latter reaches its maximum magnitude. As a consequence, the release of the OL leaves behind a higher magnitude of compressive residual strain. The effect of the compressive residual strain on the cyclic strain at the crack tip is a shift of towards lower magnitudes, as revealed by our measurements.

The strain measurement at the propagation stage "D" shows the same magnitude as the strain found prior to the OL. This proves that when the crack passes the OL site by 1mm, the compressive strain state returns back to the normal cyclic condition, as if the OL never occurred.

We note that negative strain values found in the crack wake are consistent with the strain profiles reported by Croft [30] who also used a similar experimental technique.

5.2. FEM strain state evaluation after the overload

After further validation of the elastoplastic model proposed in [a], the strain field ahead of the crack tip arising after the application of an OL could be simulated to high accuracy and with good confidence. With the purpose of understanding whether the baseline fatigue crack propagation affected the resulting strain state, we simulated both cases that we studied experimentally up to the stage when the crack reaches the propagation stage that corresponds to the cyclic load application right after the OL occurrence. To compare the strain fields between the two cases, the reference load was imposed in the model that corresponded to the minimum load reached in the R=0.7 test (i.e. F_{min}=606.7N). Strain profiles were extracted at the same crack length and load conditions corresponding to the instants shown in the Fig.1(b-c) labeled ad C and S', for R=0.7 and R=0.1, respectively.

It is evident that the introduction of an OL 'overwrites' the effect of previous cyclic material deformation: at the same load level the two strain profiles are practically indistinguishable. In view of this result, it is clear that the change in strain states that arise for the two baseline cyclic conditions immediately after the OL are indentical. This leads to an important conclusion that in both loading conditions the residual strain and stress and their influence on crack retardation are practically identical.

6. Residual stress and crack closure contributions to crack retardation

The studies of the overload effect under constant ΔK fatigue at several loading ratios $R_K=K_{min}/K_{max}$ have been previously carried out by Ishihara [34] and Borrego [35]. Whilst the former reported an enhancement of fatigue life at higher R_K, the latter observed the opposite trend. We believe that the controversy partly stems from the lack of understanding of the roles of plasticity-induced crack closure and residual stress effects, respectively.

It is reported in the literature [36] that crack closure plays an important role in affecting the growth rate if controlled loading ratio R is lower than 0.7. Our experiment confirms this, since no traces of crack closure were detected in the sample cyclically loaded at R=0.7 either by DIC or SEM fractography. The same study [36] also reported that the FCGR variation with R could be captured by the effective stress intensity factor range that is strictly related to the crack opening and closure levels. It is also worth noting that the FCGR slope in the Paris' regime does not appear to change for different loading ratios. Our test results (Table 1) agree with this observation. In the near-threshold regime of crack propagation, a more prominent effect is observed, as reported in [37], as the loading ratio varies.

Given that the crack propagation under varying loading ratio R is mainly influenced by the change in closure level, we focused our attention on the behaviour of FCGR at the occurrence of overload for different R.

6.1. Effective equivalent stress intensity factor range

Despite several minor modifications proposed in the decades since its introduction, the concept of effective stress intensity factor introduced by Elber [8] remains the most widely and generally accepted means of quantification for the principal crack driving force [38-40].

In the Paris regime of propagation, the fatigue crack growth rate dependence on the effective stress intensity factor range follows a power law relationship (2). Under the assumption that the steady-state FCGR described by (2) and shown in Fig.3 is representative of the behaviour unaffected

by the overload, we can calculate the SIF range that would give the same fatigue crack propagation rate da/dn that was observed experimentally. This can be accomplished by using the equivalent SIF range ΔK_{eq} according to Walker's formulation, which in this specific case also becomes the equivalent effective SIF, $\Delta K_{eq,eff}$. By rewriting equation (6) as

$$\frac{da}{dN} = C_0 \, \Delta K_{eq,eff}{}^{m_w}, \tag{13}$$

the totality of the experimental results can be directly superimposed onto the Paris master curve in a form independent of the load ratio R, for the purposes of comparison. Next, $\Delta K_{eq,eff}$ can be readily calculated by inversion of (13), i.e.:

$$\Delta K_{eq,eff} = \sqrt[m_w]{\frac{1}{C_0}\frac{da}{dn}} \tag{14}$$

Once the new parameter $\Delta K_{eq,eff}$ is computed using (14) for each instant of crack propagation, all the experimental points fall onto the prediction of Walker

The normalised SIF range reduction ratio ("knock-down" multiplier) due to the overload and its consequences can be evaluated through the normalised ratio β expressed in terms of the effective $\Delta K_{eq,eff}$ computed above, and the equivalent SIF range ΔK_{eq} corresponding to each experimental point evaluated by means of (4).

$$\beta = \frac{\Delta K_{eq} - \Delta K_{eq,eff}}{\Delta K_{eq,eff}} \tag{15}$$

This ratio represents the reduction in the equivalent stress intensity factor range from the unaltered one following the overload occurrence. With the purpose of comparing the outcomes from the tests

at R=0.1 and R=0.7, the variation of reduction ratio β was considered, and found to be fitted well with a log-normal function given by:

$$\beta = \frac{\emptyset}{\sigma\, a' \sqrt{2\,\pi}} \exp\left(-\frac{(\log a' - \mu)^2}{2\,\sigma^2}\right) \tag{16}$$

Here a' is the local crack extension length defined from the OL site, and $\emptyset, \mu$ and σ are the fitting parameters which define respectively its amplitude, skewness and width. Fitting was performed for the two data sets to obtain the parameter values for $\beta_{R=0.1}$ and $\beta_{R=0.7}$.

Since the goal of the present work is the attempt to distinguish the contribution of residual stress and crack closure in crack growth retardation, parameter β can be used as a measure of the durability of contribution to OL retardation from each mechanism. For the case of R=0.7, the only active mechanism is residual stress, while at R=0.1 a combination of residual stress with crack closure is present. It is worth mentioning that crack arrest was observed in the case of R=0.7. At this stage, before the crack started propagating again, the value of $\beta_{R=0.7}$ became infinite, and therefore is no longer comparable with the$\beta_{R=0.1}$.

FE simulation of the strain state generated by the application of the OL revealed that is was not significantly affected by the conditions of cyclic propagation that occurred earlier. Based on this important observation we assume from this point onwards that the residual stress influence on the crack growth retardation is the same for the two load ratio conditions examined.

In order to deconvolve the contribution of crack closure mechanism from its combination with residual stress at R=0.1, the curve for $\beta_{R=0.7}$ was subtracted from that for $\beta_{R=0.1}$ according to equation (17). In adopting this additive description of the two effect we are aware of the fact that the interaction between crack closure and residual stress may be complex, and may require more intricate approach to capture it correctly. However, it appears to offer the most suitable first approximation.

The additive decomposition that was applied only within the range of states when both cracks at R=0.1 and R=0.7 were propagating, i.e. da/dn ≠0, led to the expression:

$$\beta_{\text{closure}} = \beta_{R=0.1} - \beta_{R=0.7} \tag{17}$$

Figure 9 below presents the experimental data points, curve fits and the closure contribution evaluated using equation (17).

The dashed vertical line denotes the plastic zone boundary according to the following relation from linear elastic fracture mechanics:

$$r_p = \gamma \left(\frac{K_{max}}{\sigma_y} \right)^2, \tag{18}$$

where coefficient ?? is a parameter dependent on the sample thickness and on the stress-strain response of the material. Under the assumption of elastic-perfectly plastic material behaviour, this coefficient can be readily computed using the equation given below [41]. It has been noted [42] that the adoption of this formulation finds satisfactory agreement with three-dimensional numerical simulation, which leads to:

$$\gamma = 0.35 - \frac{0.29}{1 + \left[1.08 \frac{K_{max}^2}{t\,\sigma_y^2} \right]^{2.15}} \tag{19}$$

Using the value of α according to (19) in equation (18), the plastic zone radius was found to be ~2.8mm.

7. Discussion

The introduction of the stress intensity factor reduction ratio β has allowed the quantification of the retardation effect in terms of the effective equivalent SIF range variation past the OL. For comparison, the evaluation of this parameter was conducted for both load ratio conditions (R=0.1, R=0.7). The experimental data was then fitted with the log-normal function, with the purpose of subsequently subtracting the results from each other and attempting the discrimination of the two contributions. As a consequence of this analysis, the contribution from crack closure could be assessed, as shown by the dashed curve in Fig.9. The maximum contribution to retardation from the crack closure mechanism is found to occur at the distance of half the plastic zone size (i.e. $a' \cong r_p/2$). It is also worth noting that although the magnitude of the crack closure effect is comparable in magnitude with the residual stress one, the crack closure effect persists to greater crack lengths compared to the shorter acting residual stress effect that fades in magnitude within approximately half the size of the plastic zone, when the crack closure effect reaches its maximum.

Some conclusions can be drawn regarding the persistence length of each of the two crack retardation mechanisms. The sample tested at R=0.1 showed a persistent retardation effect even at crack extensions well in excess of the plastic zone size. This is likely to be related to the size of the plastic zone created by the overload that exceeds significantly the reversed plastic zone size [3]. In contrast, the sample cyclically loaded at R=0.7 manifested FCGR retardation limited only to a fraction of the plastic zone size. As confirmed by DIC analysis and fractography, plasticity-induced crack closure was not operative for this sample, and thus the crack retardation effect only caused by residual stress has a much shorter persistence length compared to the clack closure mechanisms.

For the load ratio R=0.1, following the OL, the crack tip experienced an effective equivalent SIF range reduction by up to 37% followed by its gradual restoration to the steady state condition. For the sample tested at R=0.7, after crack re-nucleation, an immediate drop of around 27% in the effective SIF range was seen, which subsequently quickly returned to the steady state value at

distances less than 1.3mm from the OL location, corresponding to about half of the OL plastic zone extent.

It is also worth noting that right after the application of the OL (instant "C" in Fig.1), experimental strain measurement indicated a drop in magnitude compared to the unaltered condition "B". This decay of strain magnitude is imputed to the effect of compressive residual stress induced by the high plastic deformation occurred at the crack tip which, in turns, changed the mean strain level during the cycling load toward lower values. This confirms the hypothesis that residual stress in this test case (R=0.7) is indeed the main reason for the effective SIF reduction. The change in strain magnitude was then compared with the one experienced at load ratio R=0.1 by means of elasto-plastic FEM simulations. It turned out that the cyclic load occurring prior the OL does not have a significant effect on the strain field alteration ahead the crack tip. Therefore, the residual strain field involved in the crack retardation can be considered equivalent for both the load cases.

DIC analysis of crack opening displacement revealed the level of crack closure before and after the occurrence of the OL. It was found that crack closure was already operative prior to the OL application, but at a lower level compared to that seen after the OL. It is important to highlight that before the OL application crack closure gradually reduces with the distances behind the crack tip. Indeed, at 0.4mm behind the tip, crack closure was barely detectable. It is worth mentioning that the plastic radius at this instant (prior OL) was of around 1mm. Quantification of these values could be made by looking at the effective SIF range that showed a drop of around 35% at 0.55mm from the OL site in the case of R=0.1. This value exceeds the influence of the solely the crack closure effect, β_{closure}. However, this difference can be expected, explained by the fact that DIC analysis is only able to assess the closure at sample free surface. This implies that the closure level assessed with DIC may have an error, since it neglects the gradient of closure level that occurs in the bulk, where the plane stress condition gradually evolves to the plane strain state.

In other words, the retardation contributions due to crack closure and residual stress for two different load cases were each independently verified using alternative independent techniques (XRD/FEM and DIC), showing satisfactory agreement.

Considerations reported above lead to the conclusion that the residual stress ahead the crack tip is operating solely within a region confined to about half the size of the plastic zone generated by the overload. In contrast, crack closure is an effect that persists longer following OL. For low load ratios, plasticity-induced crack closure affects FCGR immediately once the crack moves past the overload site.

8. Conclusions

The role of plasticity-induced crack closure and residual stress/strain on crack retardation after occurrence of overload has been studied. Several techniques adopted for the investigation of this phenomena turned out to be complementary in helping understand the two mechanisms operating.

In order to separate the two contributions, fatigue samples were loaded at high load ratio (R=0.7) at which crack closure was inhibited. This allowed the investigation of residual stress as the main cause of crack retardation. The comparison with the sample tested at R=0.1 permitted the analysis of fatigue crack growth rate effect in combination with crack closure.

Crack closure was additionally characterised for both samples using DIC and fractography tools. Both techniques confirmed that crack closure operated solely in the sample at R=0.1. Also, fractography analysis highlighted the regions where crack flank contact occurred.

The residual strain induced by overload in the sample loaded at R=0.7 was studied using synchrotron X-ray powder diffraction SXRPD. The conclusion was drawn from the strain maps that immediately following the overload, the crack tip experienced a reduction of the strain value magnitude, due to induced compressive residual strain. Further measurement at 1mm past the overload showed that the mean stress intensity factor was completely restored.

A new parameterβ, the SIF reduction ratio, was introduced. It describes the relative reduction of the equivalent SIF range, and allows appreciating the effect of residual strain only, and also in combination with crack closure. It was found that residual stress alone slows down the crack growth within a distance from OL site equal to approximately half of the plastic zone size due to the overload. This reduction of the SIF range is in good agreement with the results of SXRPD. On the other hand, the addition of the crack closure effect in the R=0.1 sample meant that the persistence length of the OL was similar to the plastic zone size.

The separation of the two effects was sought by means of fitting functions, and allowed clear identification of the crack closure persistence length. It is now possible to conclude that, despite inaccuracies that may arise from data scatter and fitting, it is possible to conclude that the crack closure contribution becomes active immediately upon the crack advances past the OL location, and reaches its maximum effectiveness at the same time as the residual stress effect vanishing, around half the plastic zone size. The SIF range reduction ratios evaluated by DIC and SXRPD techniques were in good agreement with the values assessed using the normalised effective SIF (β).

The present study considered a Mg alloy as a test case for the reduction factor assessment. It is clear that this approach can also be applied to other ductile materials. It can be expected to find a variation in the extent and magnitude of the two contributions for other materials. This is likely to depend primarily upon the intrinsic characteristics, such as ductility and hardening behaviour, that govern the monotonic and cyclic plastic deformation, and thereby the plasticity induced crack closure and residual stress.

The separation of contributions from closure and residual stress are of great significance in the context of crack growth prediction in variable amplitude fatigue. Existing models [43-44] are unable to capture this effect, since they simply assume that the modified plastic zone induced by OL corresponds to the extent of crack retardation. However, as demonstrated in the present study, crack closure effect may have the prevailing role in longer term crack retardation. Furthermore, it has been shown that its occurrence is directly linked with the load ratio of prior fatigue crack

growth, rather than with the OL plastic zone size. Further studies ought to address the challenge of introducing a mathematical description of these contributions into analytical and numerical models of OL crack retardation.

Acknowledgement

AMK acknowledges funding received for the MBLEM laboratory at Oxford through EU FP7 project iSTRESS (604646). The authors declare no conflict of interest.

References

[1] R.C. Rice, R.I. Stephens. Overload Effects on Subcritical Crack Growth in Austenitic Manganese Steel. ASTM Special Technical Publication (1972), Pages 95-114

[2] R.E. Jones. Fatigue Crack Growth Retardation after single-cycle peak overload in Ti-6Al-4V Titanium alloy. Eng. Fracture Mechanics, (1973), Vol.5 pp. 585-604. Pergamon Press.

[3] R.L. Carlson, G.A. Kardomateas and P.R. Bates. The effects of overloads in fatigue crack growth. International Journal of Fatigue 13 No. 6 (1991) pp 453-460

[4] K. Sadananda, A.K. Vasudevan, R.L. Holtz, E.U. Lee. Analysis of overload effects and related phenomena. International Journal of Fatigue 21 (1999) S233–S246.

[5] R. Sunder, A. Andronik, A. Biakov, A. Eremin, S. Panin, A. Savkin. Combined action of crack closure and residual stress under periodic overloads: A fractographic analysis. International Journal of Fatigue xxx (2015) xxx–xxx International Journal of Fatigue (2015)

[6] J.M. Vasco-Olmo, F.A. Díaz, E.A. Patterson. Experimental evaluation of shielding effect on growing fatigue cracks under overloads using ESPI. International Journal of Fatigue xxx (2015) xxx–xxx

[7] S.Y. Lee, P.K. Liaw, H. Choo, R.B. Rogge. A study on fatigue crack growth behaviour subjected to a single tensile overload. Part I. An overload-induced transient crack growth micromechanism. Acta Materialia 59(2011) 485-494.

[8] W. Elber. Fatigue Crack Closure Under Cyclic Tension. Engineering Fracture Mechanics (1970) Vol2, pp.37-45. Pergamon Press.

[9] A.M. Korsunsky, X. Song, J. Belnoue, T. Jun, F. Hofmann, P. F.P. De Matos, D. Nowell, D. Dini, O. A. Blanco, M. J. Walsh. Crack tip deformation fields and fatigue crack growth rates in Ti–6Al–4V. International Journal of Fatigue 31 (2009) 1771–1779

[10] E.Salvati, S. O'Connor, T. Sui, D. Nowell, A.M. Korsunsky. A study of overload effect on fatigue crack propagation using EBSD, FIB–DIC and FEM methods. Engineering Fracture Mechanics (2016)

[11] A. Steuwer, M. Rahman, A. Shterenlikht, M.E. Fitzpatrick, L. Edwards, P.J. Withers. The evolution of crack-tip stresses during a fatigue overload event. Acta Materialia 58 (2010) 4039–4052

[12] P. Lopez-Crespo, A. Steuwer, T. Buslaps, Y.H. Tai, A. Lopez-Moreno, J.R. Yates, P.J. Withers. Measuring overload effects during fatigue crack growth in bainitic steel by synchrotron X-ray diffraction. International Journal of Fatigue 71 (2015) 11–16

[13] V. Tvergaard. Effect of underloads or overloads in fatigue crack growth by crack-tip blunting. Engineering Fracture Mechanics 73 (2006) 869–879

[14] E. Salvati, S. O'Connor, D. Nowell, A.M. Korsunsky. EBSD Investigation of Fatigue Crack Propagation Past a Crack Closure Due to Overload. The 5th International Conference on Crack Paths (CP 2015), 16-18 Sept. (2015), Ferrara, Italy

[15] M.A. Meggiolaro, A.C.O. Miranda, J.T.P. Castro, L.F. Martha. Crack retardation equations for the propagation of branched fatigue cracks. International Journal of Fatigue 27 (2005) 1398–1407

[16] D.G. Pavlou, N.V. Vlachakis, M.G. Pavlou, V.N. Vlachakis. Estimation of fatigue crack growth retardation due to crack branching. Computational Materials Science 29 (2004) 446–452

[17] L. Lawson, E.Y. Chen, M. Meshii. Near-threshold fatigue: a review. International Journal of Fatigue 21 (1999) S15–S34

[18] M. Croft, V. Shukla, N.M. Jisrawi, Z. Zhong, R.K. Sadangi, R.L. Holtz, P.S. Pao, K. Horvath, K. Sadananda, A. Ignatov, J. Skaritka, T. Tsakalakos. Mapping and load response of overload strain fields: Synchrotron X-ray measurements. International Journal of Fatigue 31 (2009) 1669–1677

[19] E. Salvati, T. Sui, H. Zhang, A. J.G. Lunt, K. S. Fong, X. Song and A. M. Korsunsky. Elucidating the Mechanism of Fatigue Crack Acceleration Following the Occurrence of an Underload. (2016) Advanced Engineering Material. In Press.

[20] K. Walker. The effect of stress ratio during crack propagation and fatigue for 2024-T3 and 7075-T6 aluminium. In> Rosenfeld M, ed. Effects of Environment and Complex Load History on Fatigue Life, ASTM STP 462. 1970, 1-4.

[21] Y. Murakami. Stress Intensity Factors Handbook Volume 2, Pergamon Press (1987)

[22] N. E. Dowling, C.A. Calhoun, A. Arcari. Mean stress effects in stress-life fatigue and the Walker equation. Fatigue and Fracture of Engineering Materials and Structures. Volume 32, Issue 3, 2009, Pages 163-179

[23] P. Livieri, E. Salvati, R. Tovo. A non-linear model for the fatigue assessment of notched components under fatigue loadings. International Journal of Fatigue, Volume 82, Part 3, January 2016, Pages 624-633

[24] I. H. Onn, N. Ahmad and M. N. Tamin. Fatigue characteristics of dual-phase steel sheets. Journal of Mechanical Science and Technology 29 (1) (2015) 51-57

[25] J. Zheng And B. E. Powel. A Method To Reduce The Scatter In Fatigue Crack Growth Rate Data. Futigue Fruct. Engng Mater. Struct. Vol. 20, No. 9, pp. 1341-1350, 1997.

[26] J. A. R. Duran, R. M. Boloy, R. R. Leoni. Some remarks on the engineering application of the fatigue crack growth approach under nonzero mean loads. Front. Mech. Eng. 2015, 10(3): 255–262 DOI 10.1007/s11465-015-0342-1

[27] D. Nowell, P.F.P de Matos. Application of digital image correlation to the investigation of crack closure following overloads. Procedia Engineering 2 (2010) 1035–1043

[28] C. Eberl. Digital Image Correlation and Tracking (Software). Web site (Nov.2015): http://www.mathworks.com/matlabcentral/fileexchange/12413-digital-image-correlation-and-tracking

[29] P.F.P. de Matos, D. Nowell. The influence of the Poisson's ratio and corner point singularities in three-dimensional plasticity-induced fatigue crack closure: A numerical study. Int. Journal of Fatigue 30 (2008) 1930–1943

[30] B. Lê Minh, M.H. Maitournam, V. Doquet. A cyclic steady-state method for fatigue crack propagation: Evaluation of plasticity-induced crack closure in 3D. International Journal of Solids and Structures 49 (2012) 2301–2313

[31] P.F.P. de Matos, D. Nowell. Experimental and numerical investigation of thickness effects in plasticity-induced fatigue crack closure. International Journal of Fatigue 31 (2009) 1795–1804

[32] M. Croft, N.M. Jisrawi, Z. Zhong, R.L. Holtz, K. Sadananda, J.R. Skaritka, et al. Fatigue history and in situ loading studies of the overload effect using high resolution X-ray strain profiling. International Journal of Fatigue (2007);29.

[33] J. P. Belnoue, T.-S. Jun, F. Hofmann, B. Abbey, A. M. Korsunsky. Evaluation of the overload effect on fatigue crack growth with the help of synchrotron XRD strain mapping. Engineering Fracture Mechanics 77 (2010) 3216–3226.

[34] S. Ishihara, A.J. McEvily, T. Goshima, S. Nishino, M. Sato. The effect of the R value on the number of delay cycles following an overload. Int. Journal of Fatigue 30 (2008) 1737–1742

[35] L.P. Borrego, J.M. Ferreira, J.M. Pinho da Cruz, J.M. Costa. Evaluation of overload effects on fatigue crack growth and closure. Eng. Fracture Mechanics 70 (2003) 1379–1397

[36] H.Tsukuda, H.Ogiyama and T.Shirais. Fatigue crack growth and closure at high stress ratios. Fatigue Fruct. Engng Mnter. Struct. Vol. 18, No. 4, pp.503 -514, 1995

[37] M.L. Zhu, F.Z. Xuan, S.T. Tu. Effect of load ratio on fatigue crack growth in the near-threshold regime: A literature review, and a combined crack closure and driving force approach. Engineering Fracture Mechanics 141 (2015) 57–77

[38] D. F. Martelo, M. D. Chapetti. Analysis of the importance of the crack closure in the driving force, for the fatigue crack growth in metastable austenitic stainless steels. Procedia Materials

Science 9 (2015) 387 – 395. International Congress of Science and Technology of Metallurgy and Materials, SAM – CONAMET 2014

[39] R. Sunder. A unified model of fatigue kinetics based on crack driving force and material resistance. International Journal of Fatigue 29 (2007) 1681–1696

[40] I. R. Wallhead, L. Edwards. A study of crack closure using the optical method of caustics and consequences for the use of dkeff as a fatigue crack driving force. Engineering Fracture Mechanics Vol. 60, No. 3, pp. 291-302, 1998

[41] H. Xiaoping, T. Moan, C. Weicheng. An engineering model of fatigue crack growth under variable amplitude loading. International Journal of Fatigue 30 (2008) 2–10

[42] M. Mehrzadi, F. Taheri. A material sensitive modified wheeler model for predicting the retardation in fatigue response of AM60B due to an overload. International Journal of Fatigue 55 (2013) 220–229

[43] B.K.C. Yuen, F.Taheri. Proposed modifications to the Wheeler retardation model for multiple overloading fatigue life prediction, International Journal of Fatigue 28 (2006) 1803-1819

[44] E. Salvati, H. Zhang, K. S. Fong, R. J.H. Paynter, X. Song, A. M. Korsunsky. Fatigue and Fracture behaviour of AZ31b Mg alloy plastically deformed by Constrained Groove Pressing in the Presence of Overloads. 21st European Conference on Fracture, ECF21, 20-24 June 2016, Catania, Italy. In: Structural Integrity Procedia.

Tables

Table 1. Paris' law parameters

Loading Ratio R	C [m/(cycle MPa √m)]	m
0.1	1.91×10^{-10}	3.21

0.7	1.76×10^{-9}	2.71

Figures

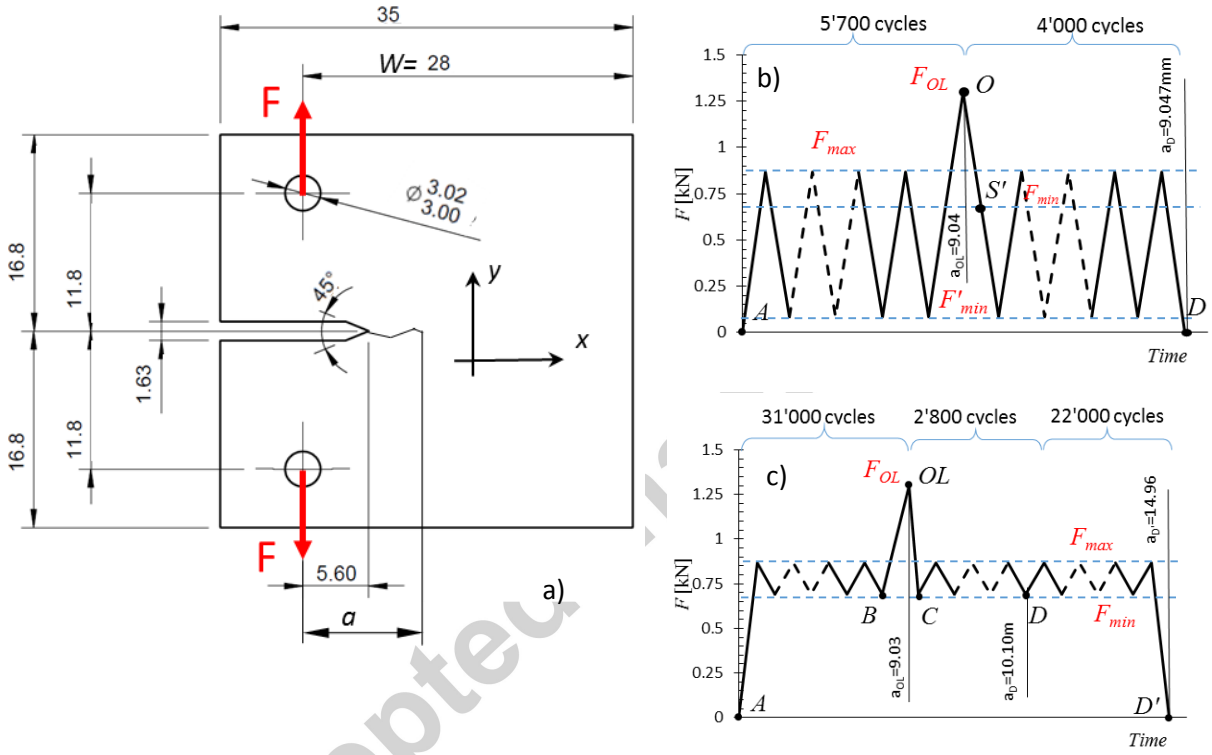

Fig.1. (a) Sample geometry (dimensions in mm), and loading history for (b) sample with R=0.1, and (c) R=0.7.

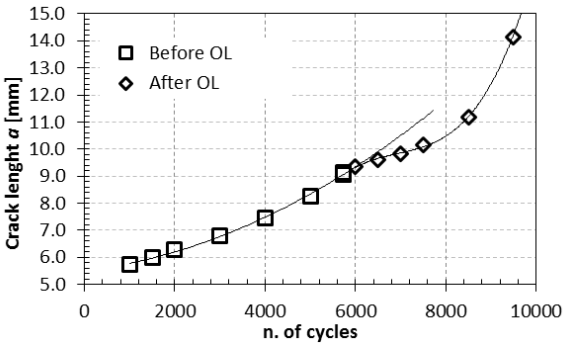

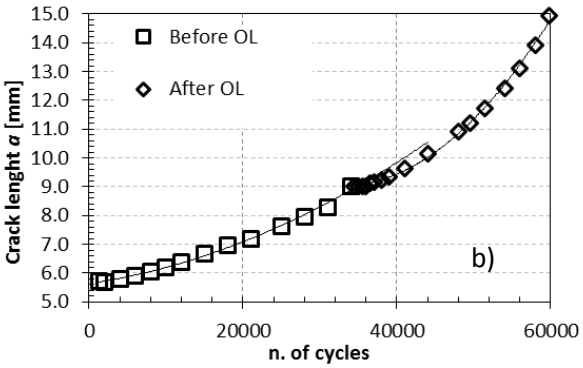

a)

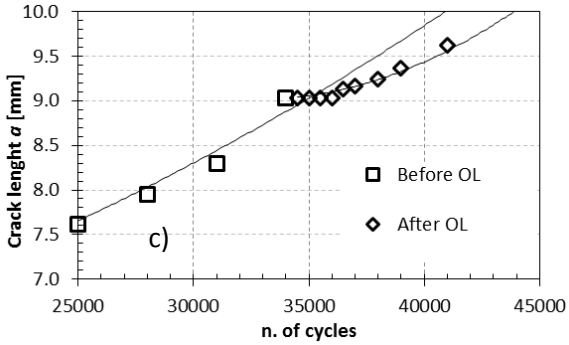

Fig.2. Crack propagation during fatigue tests at a) R=0.1, b) R=0.7 and c) R=0.7 crack arrest detail. Fitting results are reported in Fig.3 along with the FCGR values obtained from experimental tests.

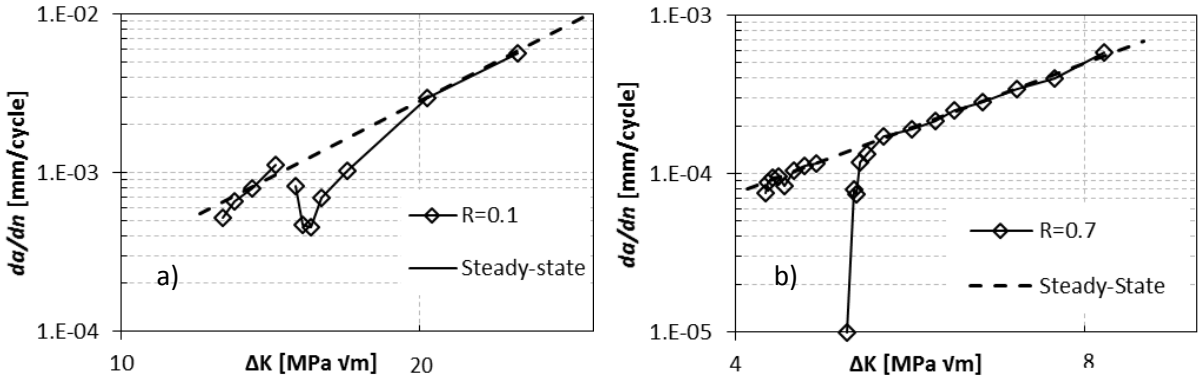

Fig.3. Fatigue Crack Growth Rate diagrams. a) R=0.1 b) R=0.7

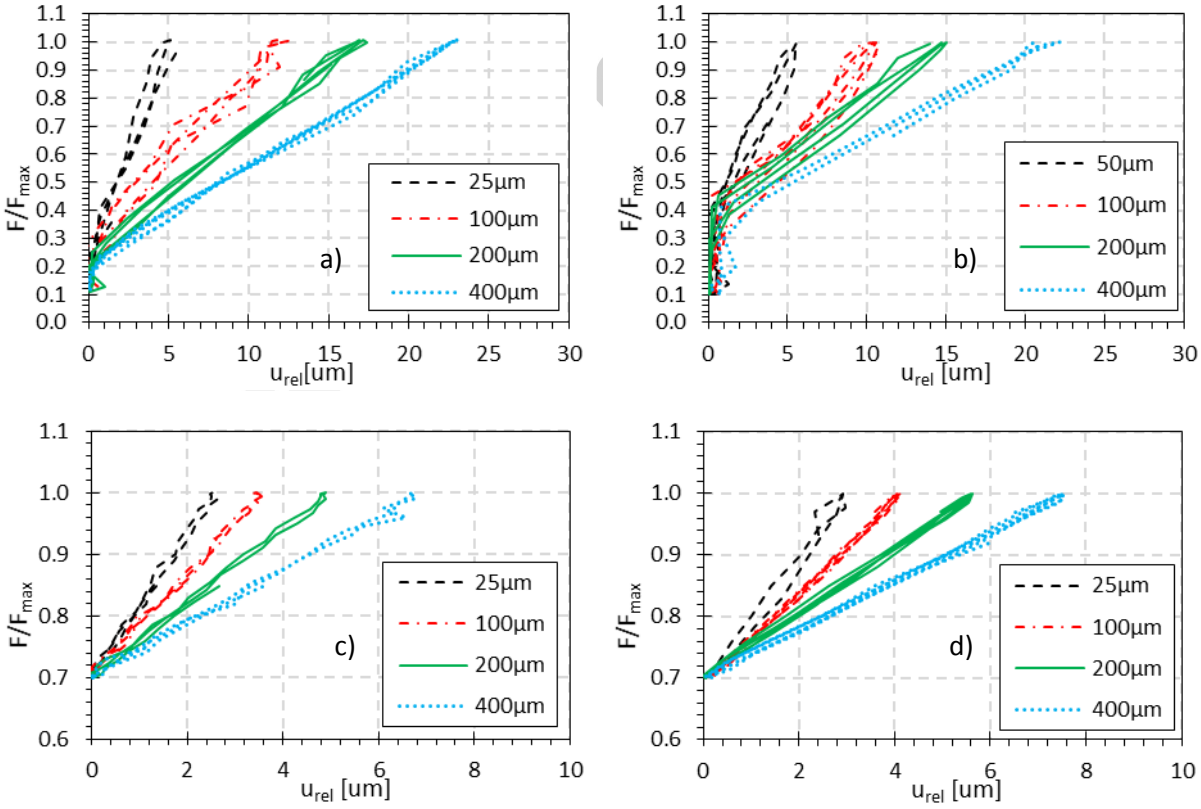

Fig.4. Crack flank relative displacement as function of the applied external load. The n.4 plots of each graph represent the trend at different distances from the crack tip towards the sample notch. Before (a) and after (b) the OL at R=0.1. Before (c) and after (d) the OL at R=0.7.

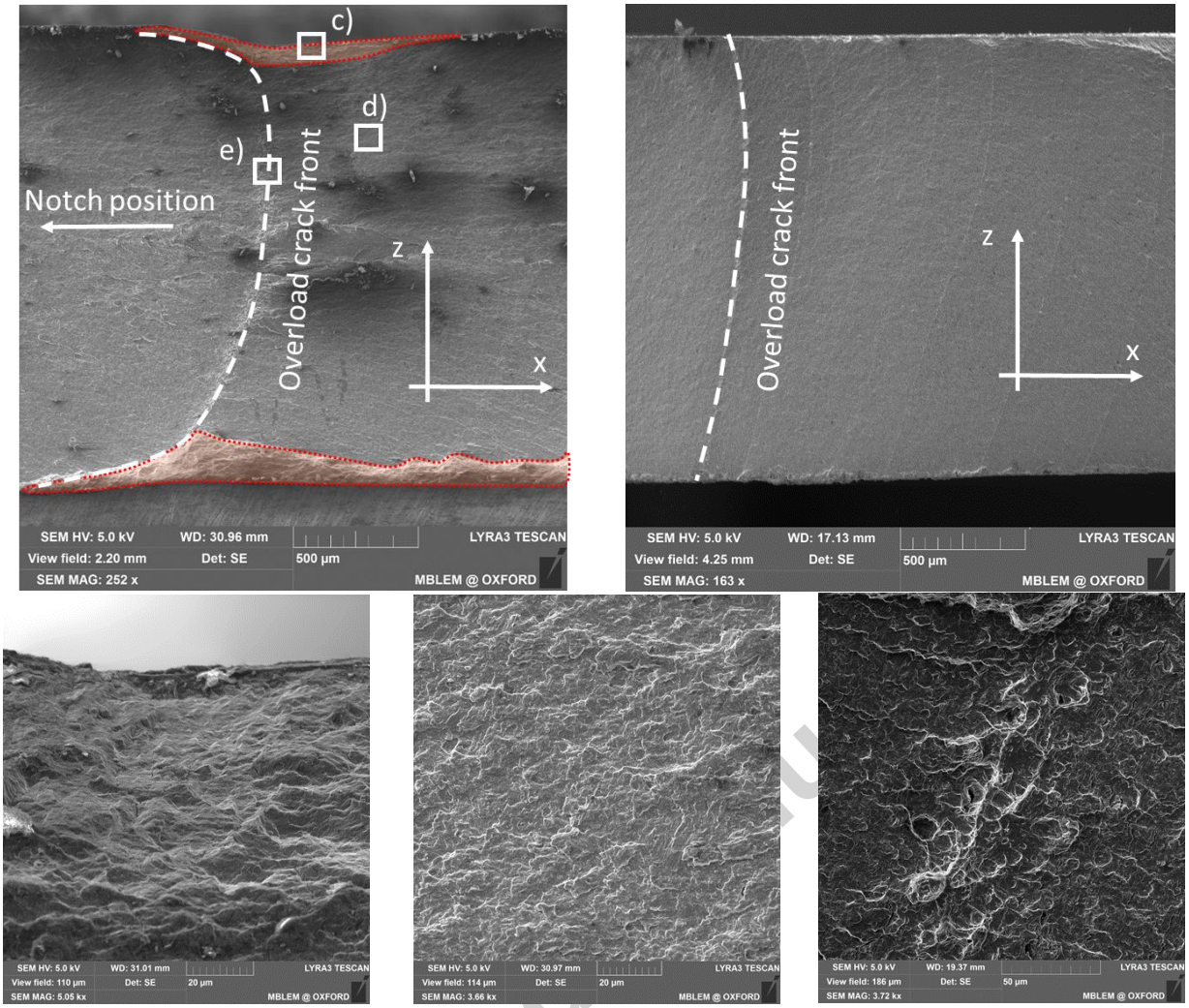

Fig.5. Crack surface SEM fractography. a) Overview image of the overload site (R=0.1). b) Overview at the OL site (R=0.7). c) Crack Closure detail (R=0.1). d) Surface detail (R=0.1). e) Overload site detail (R=0.1)

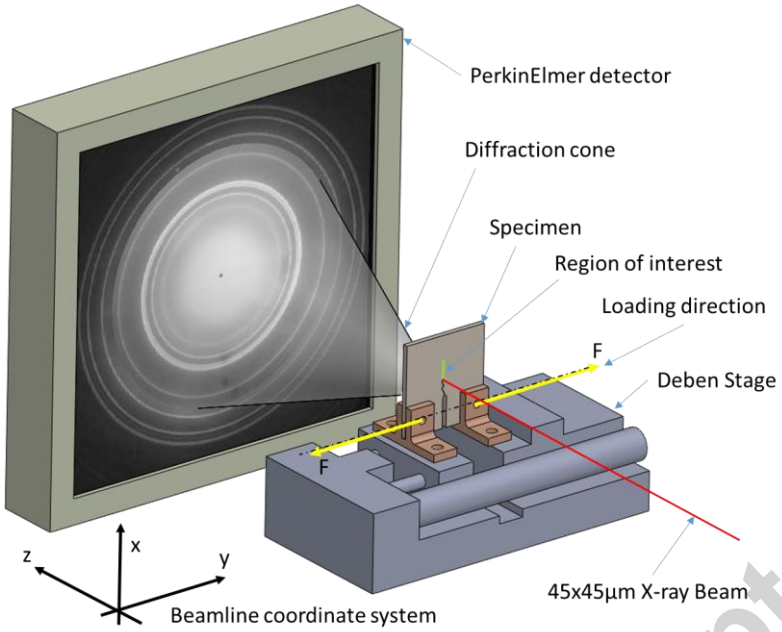

Fig.6. X-ray Synchrotron Powder Diffraction setup in trasmission mode

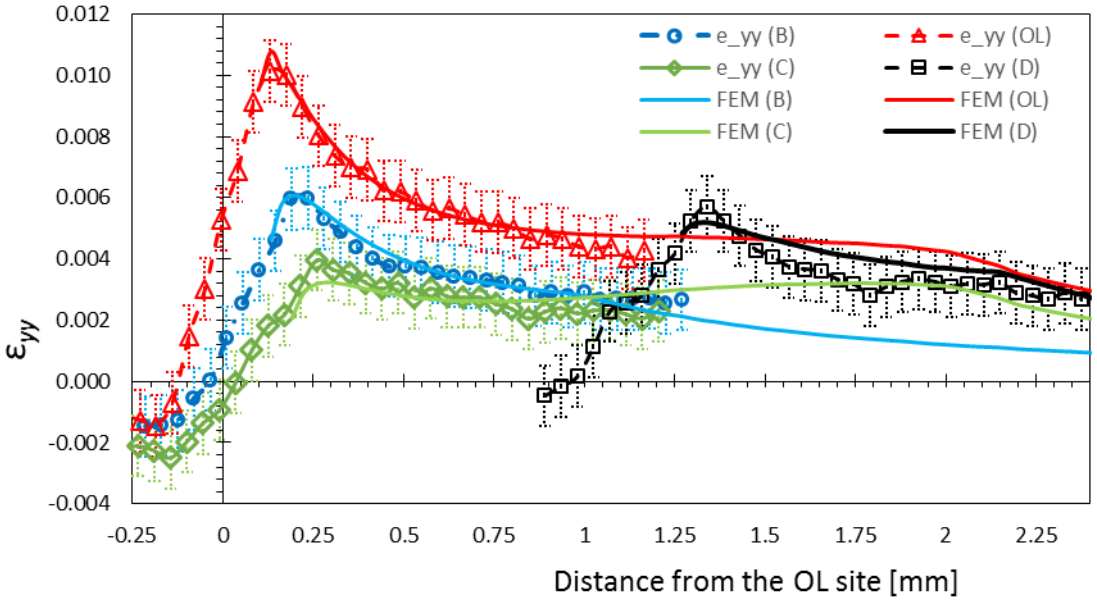

Fig.7 Strain profiles (yy component) along the crack bisector at various crack propagation stages.

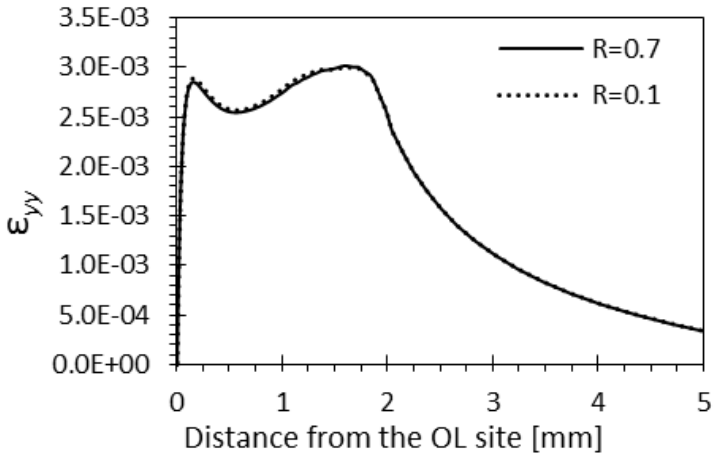

Fig.8. Strain field plot along the crack propagation direction at the propagation stage and load indicated as S and S' in Fig.1b and Fig.1c.

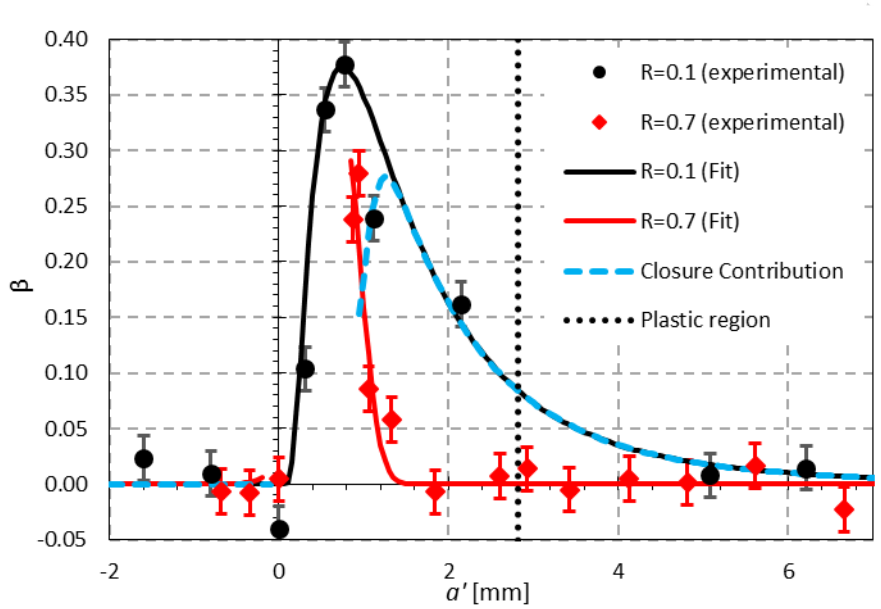

Fig.9. SIF reduction ratio β for a) R=0.1 ($\beta_{R=0.1}$) and b) R=0.7 ($\beta_{R=0.7}$)

Highlights

- Direct observation of crack opening reveals that high load ratio (R=0.7) inhibits crack closure during fatigue crack propagation
- The effect of the residual stress-strain field generated during overload vanishes when the crack tip advances beyond the overload plastic zone
- When operative, the crack closure mechanism has a longer lasting retardation effect on the crack growth rate than residual stress